LA-UR-01-1276
*Approved for public release; distribution is unlimited.*

*Title:* **DYNAMIC DEFORMATION AND DAMAGE IN CAST g-TIAL DURING TAYLOR CYLINDER IMPACT: EXPERIMENTS AND MODEL VALIDATION**

*Author(s):* G.T. (Rusty) Gray III, P.S. Steif, and T.M. Pollock

*Submitted to:*

http://lib-www.lanl.gov/la-pubs/00367088.pdf

# DYNAMIC DEFORMATION AND DAMAGE IN CAST γ-TIAL DURING TAYLOR CYLINDER IMPACT: EXPERIMENTS AND MODEL VALIDATION

G.T. (Rusty) Gray III[*], P.S. Steif[#], and T.M. Pollock[+]

*Materials Science and Technology, Los Alamos National Laboratory Los Alamos, NM 87545
# Dept. of Mechanical Engineering, Carnegie Mellon University, Schenley Park, Pittsburgh, PA 15213
+ Materials Science and Engineering, University of Michigan, 2300 Hayward Street HH Dow 2042, Ann Arbor, MI 48109

## Abstract

The dynamic deformation, damage evolution, and cracking in two cast gamma titanium aluminide alloys has been investigated experimentally and theoretically. The purpose of this study was to create and validate experimentally a finite-element model of the high speed impact of a cylindrical γ−TiAl projectile into a steel block in order to evaluate the accuracy of γ constitutive properties used in FEA simulations. In this paper the damage evolution, cracking, and validation of the constitutive response of Ti-48-2-2 and WMS cast gamma alloys is discussed. The utility of validating the high-rate impact behavior of engineering aerospace materials using Taylor cylinder impact testing is detailed.

## Introduction

Robust material models capturing the physics of high-rate material response are required for large-scale finite-element simulations of complex engineering problems of interest to the engineering implementation of intermetallics into structural applications. This includes aerospace impacts (foreign-object damage(FOD)), high-rate manufacturing processes such as high-rate forging, and armor/anti-armor interactions. Simulations of large-scale dynamic events such as ballistic impact or foreign-object damage are challenging engineering problems where materials properties under extreme conditions (large strain, high strain rates, and high temperatures) are critically important. The scientific expression of these needs is in the further development of constitutive relations that are based on established physical mechanisms and extensive experimental testing.

Implementation of the constitutive response of a material into large-scale finite-element analysis (FEA) codes for use in simulating an engineering problem of interest, such as FOD, is accomplished using a phenomenological analytic description capturing the constitutive response in a constitutive strength model. In recent years the effects of impact damage on the structure/property relationships in γ-TiAl has received focused attention in the literature due to its potential ramifications on future use of TiAl in jet engine applications[1-5]. These studies have primarily focused on the assessment of how prior impact events on TiAl can affect subsequent mechanical response. Utilization of the insights into damage evolution in γ-TiAl due to impact events afforded by these studies into large-scale engineering simulations of FOD now requires integration of damage into FEA codes and validation of these models.

The constitutive and shock response of γ-TiAl has been the subject of previous research[6-10]. Integration of the constitutive response of γ-TiAl into FEA codes requires a strength model that accurately captures its mechanical behavior. While a number of engineering strength constitutive models have found frequent engineering usage in both industrial and defense sectors[11], little focused work has been concentrated on modeling the constitutive response of these alloys[1]. To assess the accuracy and "robustness" of a material strength model to predict constitutive response (yielding and strain-hardening) over a wide range of loading conditions, it is critical to conduct integral experiments to validate the physics captured by the model. The strain rate dependence of the uniaxial flow strength of a material is not directly measured at intermediate strain rates, i.e., $10^4$ $s^{-1}$ to $10^6$ $s^{-1}$ by

conventional testing means. However this strain-rate regime is precisely the range of critical importance to many engineering simulations including FOD and ballistic impact. The Taylor impact test represents a readily conducted axi-symmetric integrated validation test which probes both a wide range of plastic strains (deformations up to several 100's of %) and strain rates up to $10^6$ $s^{-1}$. In Taylor cylinder impact tests the strain rate at the impact anvil will typically be in the high $10^4$ or low $10^5$ $s^{-1}$ regime initially while a short distance up the Taylor cylinder the plastic strain rate will have fallen to $10^2$ $s^{-1}$ rates, and the rear portion of the cylinder will remain elastic.

The Taylor cylinder impact test, named after G.I. Taylor[12] who developed the test to screen materials for use in ballistic applications during WW II, entails firing a solid cylinder rod of a material of interest, typically 7.5 to 12.5 mm in diameter by 25 to 40-mm in length, at high velocity against a massive and rigid target. The deformation induced in the Taylor rod due to the impact shortens the rod as radial flow occurs at the impact surface. Taylor cylinder impact testing has previously been utilized to probe both the deformation response of metals and alloys in the presence of gradients of stress, strain, and strain-rate and as a means to validate constitutive models. In this approach, the final length and cylinder profile of the Taylor sample is compared with code simulations to validate the material constitutive model implemented in a finite-element code. Comparisons with the recovered Taylor sample provide a check on how accurately the code can calculate the gradient in deformation stresses and strain rates leading to the final strains imparted to the cylinder during the impact event.

The purpose of this study was to create and validate experimentally a finite-element analysis model of the high-speed impact of a cylindrical γ-TiAl projectile into a steel block in order to evaluate the accuracy of γ constitutive properties used in Abaqus FEA simulations.

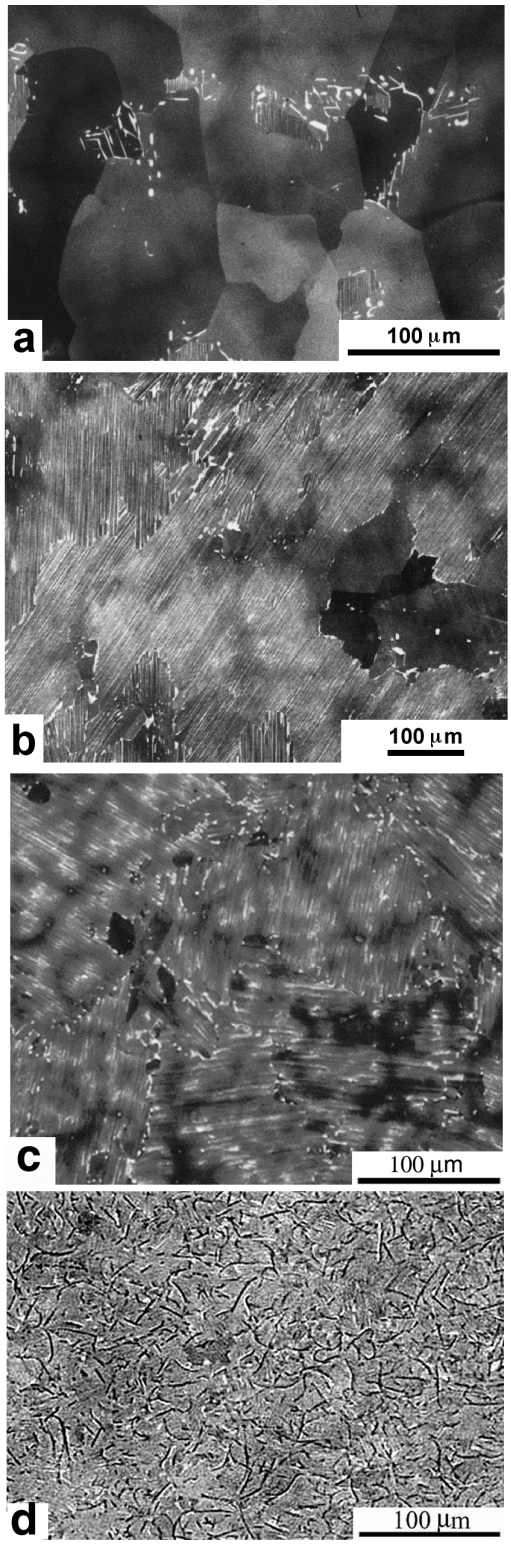


Figure 1: BSE images of the three cast γ-TiAl alloys: a) 48-2-2, b) 47-2-2, c)WMS-TiAl, and d) XD-TiAl.

## Experimental Procedure

### Materials

Three different types of cast gamma titanium aluminide alloys were utilized in this investigation. The compositions of these alloys are listed in Table I. All alloys had interstitial elements at levels typical for cast materials, with oxygen in the range of 850 – 1940 atomic ppm. The first alloy, referred to as "WMS" was selected as a representative "high strength – moderate ductility" composition. The WMS material is predominantly lamellar with a colony size of approximately 165 μm. It has a small volume fraction of equiaxed gamma grains at the colony boundaries and a fair degree of segregation remaining from the casting process. Two variations of the Ti-48Al-2Cr-2Nb class of alloys were included as "higher ductility – moderate strength" alloys. The first had a higher Al level of 47.9Al and will be referred to as "48-2-2". The second, with a lower Al level of 47.0 Al, will be referred to as "47-2-2". The 47-2-2 and 48-2-2 alloys were investment cast and heat treated at 1093°C for 5 hours, HIPed at 1205°C and 172 MPa for 4 hours, and finally heat treated at 1205°C for 2 hours. The 48-2-2 alloy had a duplex microstructure consisting of 70μm equiaxed gamma grains and approximately 6 vol.% lamellar colonies, while the 47Al alloy had a much high volume fraction of lamellar colonies with a colony size of approximately 500 μm, Figure 1.

The third alloy was produced via the "XD™" grain refinement process. It was investment cast and HIPed at 1260°C and 172 MPa for 4 hours and then heat-treated at 1010°C for 50 hours with a gas fan cool to yield a predominantly lamellar microstructure with about 1vol.% $TiB_2$ particles. This alloy is referred to as "XD-TiAl". BSE images of the microstructures of these alloys are shown in Figure 1.

**Table I** – Compositions of Cast TiAl-based Alloys (atomic %)

| Alloy | Ti | Al | Cr | Nb | Mn | W | Mo | Si | B |
|---|---|---|---|---|---|---|---|---|---|
| 48-2-2 | Bal | 47.9 | 2.0 | 2.0 | | | | | |
| 47-2-2 | Bal | 47.0 | 2.0 | 2.0 | | | | | |
| WMS | Bal | 47.3 | | 2.2 | 0.5 | 0.4 | 0.4 | 0.23 | |
| XD™-TiAl | Bal. | 44.4 | | 2.11 | 1.1 | | | | 1.09 |

**Table II** – Tensile Properties of Cast TiAl Alloys

| Alloy | Ultimate Tensile Strength (MPa) | Plastic Strains to Failure (%) |
|---|---|---|
| Ti-48-2-2 | 332 – 443 | 0.64 – 2.17 |
| WMS | 504 - 596 | 0.42 – 1.19 |
| Ti-47-2-2 | 464 - 549 | 0.63 – 1.66 |
| **45Al XD | 521 – 557 | 0.72 – 0.89 |

** Tensile properties for the XD material are from a slightly higher Al heat than utilized for the Taylor cylinder experiments

### Mechanical Behavior

The quasi-static tensile properties of the three types of TiAl alloys studied are listed in Table II. In work reported elsewhere we have shown tensile properties to vary to with cooling rates during investment casting, thus the properties are given in terms of the ranges measured for a large number of tension tests. The tensile test data reveals the 48-2-2 and 47-2-2 alloys exhibit the lowest ultimate tensile strength (UTS) and highest plastic strain to failure and the WMS-TiAl the lowest strain to failure in quasi-static tension. The WMS-TiAl and XD-TiAl both exhibit higher UTS's than the 48-2-2 alloys and their plastic strains to failure are reasonably comparable, as seen in Table II. The 45Al XD material is seen to exhibit

the highest consistent, smallest scatter, plastic strains to tensile failure albeit the 47-2-2 and the WMS-TiAl display both higher maximum and wider ranges in their strains to failure. The compressive constitutive responses of the Ti-48-2-2, WMS-TiAl, and XD-TiAl alloys were also characterized as a function of temperature and strain rate. Quasi-static compression tests were conducted at a strain rate of 0.001 $s^{-1}$. Samples for low and high-strain rate uniaxial compression were nominally 6.35 mm in diameter and had a 1:1 length-to-diameter (l:d) aspect ratio. Prior to compression testing, specimen loading faces were lubricated with molybdenum disulfide. Dynamic compression tests were conducted as a function of strain rate and temperature, utilizing a compression and tensile Split-Hopkinson Pressure Bar (SHPB)[13]. The inherent oscillations in the dynamic stress-strain curves and the lack of stress equilibrium in the specimens at low strains make the determination of yield inaccurate at high strain rates.

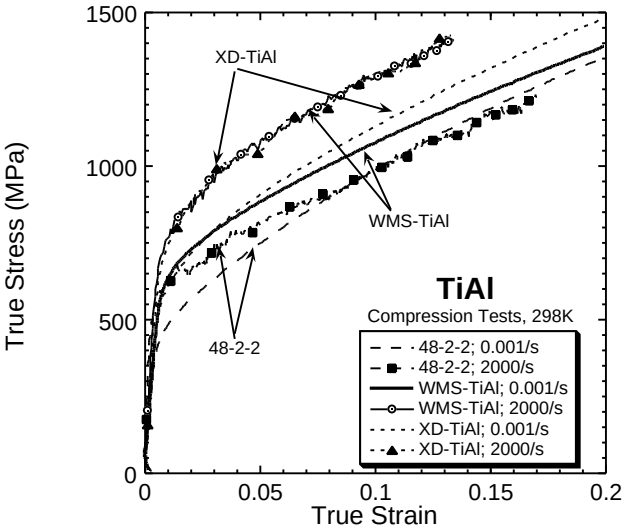


Figure 2: Compressive stress-strain response of the 3 TiAl materials studied measured at 298K at strain rates of 0.001 and 2000 per second..

The room temperature compressive stress-strain responses of the three TiAl materials at strain rates of 0.001 and 2000 /sec are presented in Figure 2. The 48-2-2 alloy is seen to display the lowest yield strength of the three aluminide materials at both strain rates. The quasi-static yield strengths of the WMS-TiAl and XD-TiAl are similar, but the XD-TiAl displays a higher work hardening rate following ~0.03 strain. At a strain rate of 2000 /sec the XD-TiAl and WMS-TiAl alloys exhibited similar stress-strain responses as seen in Figure 2.

## Constitutive and Finite-Element Modeling

To support the finite-element modeling of the Taylor cylinder tests the compressive stress-strain data for the 48-2-2 alloy was fit to the Zerilli-Armstrong(Z-A) model[14]; Figure 3 shows the compressive stress-strain data as a function of strain rate and temperature along with the Z-A modeling fit. The Z-A fit to the flow stress for the 48-2-2 material as a function of plastic strain was expressed in the form:

$$\sigma = 270 + 660\exp[-0.00350T + 0.0001750T\ln(\dot{\varepsilon})] + 3000\,\varepsilon_p^{0.96}$$

where _ is stress in MPa, $\dot{\varepsilon}$ denotes the strain rate, $\varepsilon_p$ is the plastic strain, and T is the temperature[1]. The Z-A model is observed to reasonably accurately capture the strain rate and temperature dependency of the yielding and work hardening response of the 48-2-2 alloy.

Finite-element simulations of the Taylor tests were conducted using the FEA code ABAQUS Explicit[1]. The Taylor cylinder tests for the 48-2-2 alloy were simulated as the axi-symmetrical impact of a gamma TiAl cylinder into a much larger (10 times) steel block. TiAl properties used the ZA-BCC fit shown in Figure 3. The steel block was modeled as elastic. The sides and rear face of the impacting cylinder were taken to have zero normal and shear stress. Contact between the impact face and the steel block was assumed to be frictionless; that is, the shear stress between the cylinder and the block was zero, and the normal or axial displacement was identical in the cylinder and the block. For the most refined mesh, elements of type CAX4R were used for the cylinder and block, with ~18000 elements in the cylinder and ~13000 in the steel block.

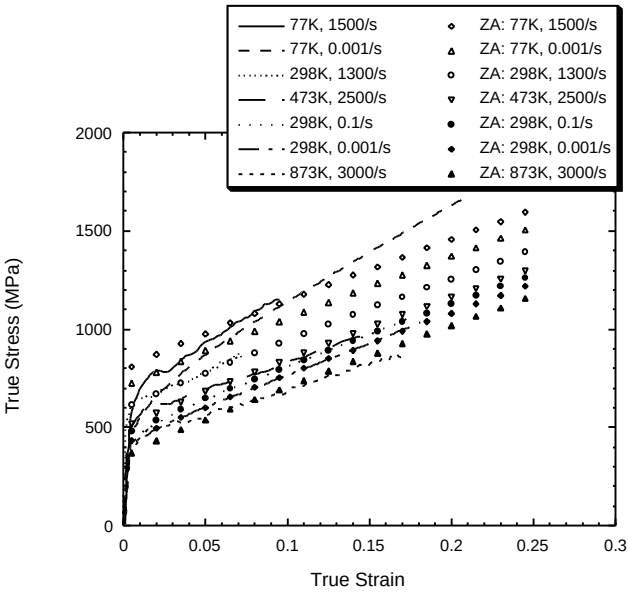


Figure 3: Stress-strain response of Ti-48-2-2 (lines) and Z-A Constitutive Modeling Fit (symbols).

## Experimental Results and Discussion

### Taylor Cylinder Tests

Photographs of the Taylor cylinders for the three intermetallics following testing are shown in Figure 4 and the impact velocities for the tests and the post-shot dimensions of the cylinders listed in Table III. Based upon observation of the deformation and cracking response of the post-test Taylor cylinders and the extent of deformation absorbed by the cylinders of the different TiAl alloys at an equivalent velocity several conclusions can be made. First the exterior surfaces of the Taylor cylinders are seen to be significantly different following testing. The surface roughness of the 47-2-2 cylinder is seen to exhibit a pronounced "orange-peel" consistent with the coarse microstructure of the cast 47-2-2 microstructure. The WMS-TiAl exhibits a reduced level of surface roughening but is still evident. The XD-TiAl cylinder surface following the 177 m/s impact displayed only slight roughening. The overall extent of deformation, change in cylinder length from the starting 2" (50.8 mm), imparted into a Taylor cylinder is most directly linked to its dynamic yield strength as previously demonstrated by many researchers[15],although not exclusively as is reflected in the difference between the 47-2-2 and WMS-TiAl alloy results. At nominally 175 m/s the XD-TiAl experienced the smallest reduction in cylinder length as seen in Table III consistent with its higher quasi-static yielding response. The other feature worthy of note is that all the Taylor cylinders exhibited isotropic plastic responses, i.e. the cylinder footprints are circular, with exception of the WMS-TiAl which displays a slightly ellipsoidal-shaped Taylor footprint. The observations of the final lengths of the 47-2-2 and WMS-TiAl cylinders are at first difficult to understand until the impacted cylinders are examined more thoroughly. Figure 5 gives a presentation of the Ti-aluminide Taylor cylinder diameters as a function of distance from the impact end of the Taylor cylinders. The 47-2-2 cylinder displays a longer percentage of the total cylinder length displaying deformation, i.e., propagation of the plastic wave up the cylinder, following the nominal 175 m/s impact compared to the WMS-TiAl cylinder. The extent of deformation as a function of distance along the cylinder is however seen to be significantly higher in the WMS-TiAl in the first 17 mm of distance from the impact interface for the Taylor cylinder sample compared to the 47-2-2 cylinder as seen in Figure 5. The more extensive nature of the deformation in the WMS-TiAl within the first 17 mm of the cylinder length, i.e. more uniform increase in cylinder diameter, accounts for the reduced length of this cylinder compared to the 47-2-2 or the XD-TiAl fired at nominally 175 m/sec. This more extensive plastic bulging response for the WMS alloy is consistent with the lower rate of quasi-static work hardening exhibited by the WMS-TiAl compared to the 47-2-2 alloy; a higher rate of work-hardening in the 47-2-2 absorbs more energy compared to a higher percentage of the WMS-TiAl cylinder being plastically deformed. More extensive propagation of the plastic deformation up the first third of the length of the Taylor cylinder in the WMS-TiAl alloy therefore leads to a larger reduction in the rod length. The importance of work-hardening behavior on plastic wave propagation up the length of a Taylor cylinder has been demonstrated previously for Zr cylinders where low work hardening related to deformation twinning can enhance the extent of plastic flow up a cylinder[15]. Whether differences in extent of deformation twinning between the WMS-TiAl and 48-2-2 materials played a role in the current results remains unclear at present.

The extent of cracking on the circumference and sides of the Taylor cylinder footprints was also observed to differ between the three gamma titanium

aluminides are listed in Table III. While impacting at ~175 m/s was observed to lead to a number of 1mm+ in length cracks in the 47-2-2 and WMS-TiAl alloys only short cracks were seen in the XD-TiAl following impact at this velocity. Accordingly, an additional cylinder of the XD-TiAl alloy was tested at 210 m/s as seen in Figure 4d.

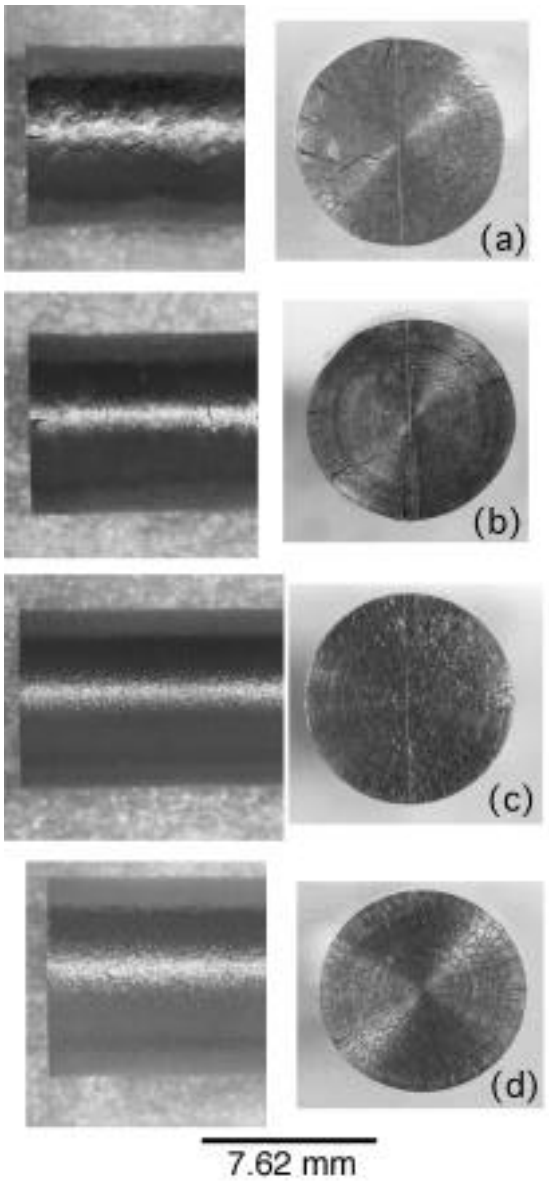


Figure 4: Side view and footprint of Taylor cylinders of: a) 47-2-2 fired at 171 m/s, b) WMS-TiAl impacted at 175 m/s, c) XD-TiAl impacted at 177 m/s, and XD-TiAl impacted at 210 m/s.

At this velocity an increase in the length of cracks formed was observed in the XD-TiAl although the crack lengths generated remained less than 50% of that formed in the 47-2-2 and ~37% of the maximum crack length formed in the WMS-TiAl. The observation of the longest cracks in the WMS-TiAl material of the three Ti-aluminides tested is consistent with the fact that the WMS-TiAl also exhibits the lowest quasi-static ductility as presented in Table II. This consistency is not surprising as cracking on the outer edges of the Taylor cylinder due to the hoop tensile stresses generated there occurs late in the Taylor formation process when the strain rates are rapidly falling and the rod is ready to rebound off the anvil. The footprint diameters of the three gamma titanium aluminides at which cracking starts is given in Table III. It is interesting to note that at this higher velocity at which the XD-TiAl begins to display longer cracks, > 0.5 mm, the outer diameter of the cylinder footprint has achieved an equivalent diameter of ~ 0.328 (8.31 mm) as that required to generate significant cracking in the 47-2-2 and WMS-TiAl alloys. This observation supports the concept of a critical stress plus strain accumulation criterion to damage evolution through cracking in the three gamma titanium aluminides studied. This further supports using a strain accumulation criterion in FEA modeling of the Taylor cylinder testing[1].

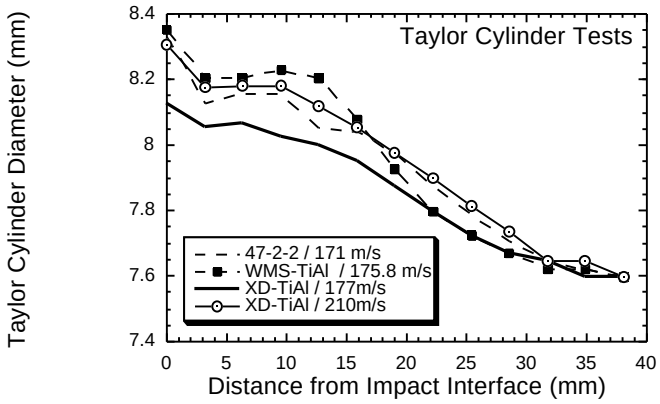


Figure 5: Plot of Taylor cylinder diameter as a function of distance from the impact footprint end of the Taylor cylinder.

FEA Modeling

FEA modeling was conducted for the Taylor cylinder test for the 48-2-2 alloy sample impacted at 167.2 m/sec. The side profile and footprint of the 167.2 m/sec 48-2-2 recovered sample is shown in Figure 6. The experimental length of the Taylor sample for the Ti-48-2-2 after rebound was measured to be 1.8835" (47.84 mm). The FEA simulation predicted a length of 1.875" (47.62 mm after rebound. Cracks appeared on the sides of the specimen up to 1.0 mm from the impacted face.

Contours of the hoop (circumferential) stress on the outer surface in the vicinity of the edge of the specimen are shown in Figure 7. The hoop stress at any single point tends to increase with time from zero and then decreases. These contours were taken at a single instant in time at which the hoop stress at most points in the region shown have reached their maximum values. One can see that the hoop stress varies from 650 MPa near the corner to below 300 MPa near the upper end of the region displayed. The accumulated plastic strain is in excess of 6% over the region displayed. Since the plastic strain is far in excess of the tensile ductility of the alloy, the extent of cracking may be controlled by the tensile stress. For example, if one presumes that 400 MPa stress (approximately the uniaxial tensile strength of this alloy) is required to induce cracking, then one would predict cracks to extend up to 0.87 mm from the bottom of the specimen. This can be compared with observed crack extent of 1.0 mm. A cracking criterion which requires both the exceeding of a critical plastic strain and a critical tensile stress has been useful in rationalizing observations and predictions of cracking due to particle impact on specimens simulating the leading edge of turbine blades.

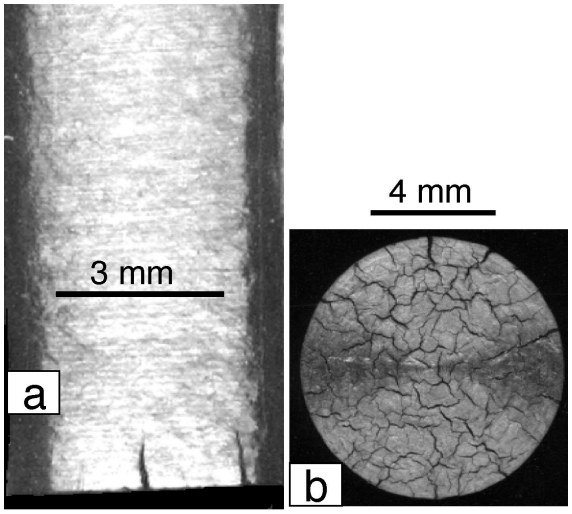


Figure 6: Taylor Cylinder of Ti-48-2-2 showing cracking along the: a) axis, and b) on the Taylor sample footprint.

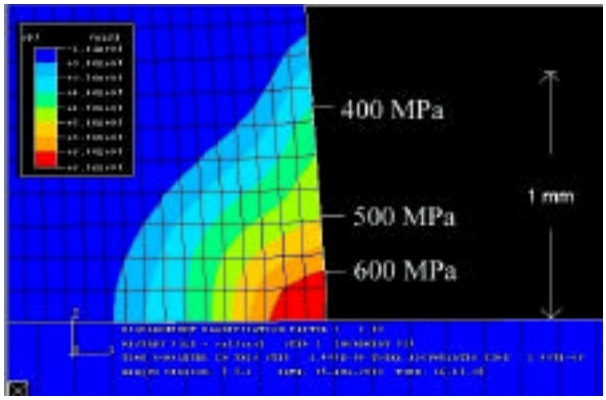


Figure 7: ABAQUS simulation of Ti-48-2-2 Taylor cylinder impacted at 167.2 m/sec.

**Table III** – Taylor Cylinder Test Data

| **Alloy** | **Taylor Test Velocity** (m/sec) | **Final Cylinder Length** (mm) | **Cylinder Diameter at Footprint** (mm) | **Number of cracks on Taylor** | **Crack Length Range on Side of Taylor Cylinder** (mm) |
|---|---|---|---|---|---|
| 48-2-2 | 167.2 | 47.84 | - | | 1mm max |
| 48-2-2 | 171.3 | 47.73 | 8.33 | 7 | 0.61 to 1.07 |
| WMS-TiAl | 175.8 | 45.95 | 8.15 / 8.35 | 6 | 0.79 to 1.47 |
| XD-TiAl | 177.3 | 48.18 | 8.13 | 4 | 0.22 to 0.36 |
| XD-TiAl | 210 | 47.32 | 8.31 | 4 | 0.27 to 0.55 |

## Conclusions

Based on a study of the constitutive behavior and Taylor impact testing of three gamma titanium aluminides the following conclusions can be drawn.

1) While the stress-strain response of the 48-2-2, WMS-TiAl, and XD-TiAl do not differ significantly in their constitutive responses the differences in yield strength, work-hardening behavior, and tensile strains to failure were found to strongly correlate with the extent of deformation and cracking during an integrated impact test event, i.e. A Taylor cylinder test. The lower work-hardening of the WMS-TiAl is seen to correlate in more extensive bulging in the first 17 mm of the Taylor cylinder compared to the 47-2-2 alloy which displayed more uniform hardening along the length of the Taylor cylinder. The XD-TiAl alloy displayed the least deformation when impacted at 175 m/sec consistent with its higher flow stress.

2) The extent of cracking in the 48-2-2, WMS-TiAl, and XD-TiAl materials during Taylor cylinder testing was observed to be generally consistent with the ranking between these alloys on the basis of their quasi-static tensile failure data. However due to the pronounced differences in yield and hardening behavior the XD-TiAl material required a significantly higher impact stress to achieve the strain level necessary to activate cracks on the circumference of the impact footprint. Even the higher impact velocity for the XD-TiAl did not lead to the same magitude or number of cracks as displayed by the 47-2-2 or WMS-TiAl.

3) Taylor cylinder impact testing provides an integrated test capable of differentiating differences between the constitutive and damage evolution behavior of gamma titanium aluminides. As such this Taylor cylinder tests provide an experimental method which can be utilized to validate engineering models of impact behavior of relevance to complex dynamic loading paths.


## Acknowledgements

The authors would like to acknowledge General Electric Aircraft Engines for providing a portion of the cast materials and P. McQuay of the Howmet Corporation for collaborations on casting. Contributions by N. Biery, R. Raban, J. Milke, V. McKenna, K. Oldham and C. Feng are also appreciated. This work was supported the AFOSR-PRET Program on Gamma Titanium Aluminides under the contract F496-95-0359. GTG III acknowledges that portions of this work was conducted under the auspices of the US Department of Energy. GTG acknowledges the contributions of M.F. Lopez and C.M. Cady to the mechanical characterization and constitutive modeling of the Ti-48-2-2 alloy, respectively and C.P. Trujillo and B. Jacquez for conducting the Taylor Anvil tests.


## References


1. P.S. Steif, M.P. Rubal, G.T. Gray III, and J.M. Pereira, "Damage in Gamma Titanium Aluminides due to Small Particle Impacts," J. Mech. Phys. Solids, 46 (1998), 2069.

2. P.S. Steif, J.W. Jones, T. Harding, M.P. Rubal, V.Z. Gandelsman, N. Biery, and T.M. Pollock: in Structural Intermetallics 1997, M.V. Nathal, R. Darolia, C.T. Liu, P.L. Martin, D.B. Miracle, R. Wagner, and M. Yamaguchi, eds., The Minerals, Metals & Materials Society, Warrendale, PA, vol. 1997, pp. 435.

3. T. Harding, J.W. Jones, T.M. Pollock, and P.S. Steif, "Room Temperature Fatigue Response of Gamma-TiAl to Impact Damage," Scripta Metall. Mater., 40 (1999), 445-449.

4. T.S. Harding and J.W. Jones, "Behavior of Gamma TiAl Subjected to Impact Damage and Elevated Temperature Fatigue," Scripta Metall. Mater., 42 (2000), 129-135.

5. T.S. Harding and J.W. Jones, "The Effect of Impact Damage on the Room Temperature Fatigue Behavior of Gamma-TiAl," Metall. & Matls. Trans., 31A (2000), 1741-1752.

6. S.A. Maloy and G.T. Gray-III, "High Strain Rate Deformation of Ti-48Al-2Nb-2Cr in the

Duplex Morphology", in Gamma Titanium Aluminides, eds. Y.-W. Kim and R. Wagner, (TMS, 1995), 307-314.

7. G.T. Gray III, "Influence of shock loading on the structure/property response of Ti-48Al-2Cr-2Nb and Ti-24Al-11Nb," Journal de Physique IV, Colloque C8 (1994), 373-378.

8. S.A. Maloy and G.T. Gray-III, "High Strain Rate Deformation of Ti-48Al-2Cr-2Nb," Acta Materialia, 44 (1996), 1741-1756.

9. G.T. Gray III: in Deformation and Fracture of Ordered Intermetallic Materials III, W.O. Soboyejo, T.S. Srivatsan, and H.L. Fraser, eds., The Minerals, Metals and Materials Society, vol. 1996, pp. 57-73.

10. Z. Jin, C.M. Cady, G.T. Gray III, and Y.-W. Kim, "Mechanical Behavior of a Fine-Grained Duplex Gamma-TiAl Alloy," Metall. & Matls. Trans., 31A (2000), 1007-1016.

11. S.R. Chen and G.T.G. III, "Constitutive behaviour of tantalum and tantalum-tungsten alloys," Metall. Trans., 27A (1996), 2994-3006.

12. G.I. Taylor, "The use of flat ended projectiles for determining yield stress. I: Theoretical considerations," Proc. R. Soc. Lond. A, 194 (1948), 289-299.

13. G.T. Gray III: in ASM Handbook - Mechanical Testing and Evaluation,, ASM International, Materials Park, OH, vol. 8, 2000, pp. 462-476.

14. G.T. Gray III, S.R. Chen, and K.S. Vecchio, "Influence of Grain Size on the Constitutive Response and Substructure Evolution of Monel 400," Metall. & Matls. Trans., 30A (1999), 1235-1247.

15. P.J. Maudlin, G.T. Gray_III, C.M. Cady, and G.C. Kaschner, "High-Rate Material Modeling and Validation Using the Taylor Cylinder Impact Test," Philos. Trans. Roy. Soc. A, 357 (1999), 1707-1729.